



**HAL**  
open science

# Modeling and simulation of VOCs removal by nonthermal plasma discharge with photocatalysis in a continuous reactor: Synergetic effect and mass transfer

Aymen Amine Assadi, Abdelkrim Bouzaza, Smail Merabet, Dominique Wolbert

## ► To cite this version:

Aymen Amine Assadi, Abdelkrim Bouzaza, Smail Merabet, Dominique Wolbert. Modeling and simulation of VOCs removal by nonthermal plasma discharge with photocatalysis in a continuous reactor: Synergetic effect and mass transfer. *The Chemical Engineering Journal*, 2014, 258, pp.119-127. 10.1016/j.cej.2014.07.050 . hal-01064033

**HAL Id: hal-01064033**

**<https://hal.science/hal-01064033>**

Submitted on 4 Nov 2014

**HAL** is a multi-disciplinary open access archive for the deposit and dissemination of scientific research documents, whether they are published or not. The documents may come from teaching and research institutions in France or abroad, or from public or private research centers.

L'archive ouverte pluridisciplinaire **HAL**, est destinée au dépôt et à la diffusion de documents scientifiques de niveau recherche, publiés ou non, émanant des établissements d'enseignement et de recherche français ou étrangers, des laboratoires publics ou privés.

# **Modeling and simulation of VOCs removal by nonthermal plasma discharge with photocatalysis in a continuous reactor: Synergetic effect and mass transfer**

ASSADI Aymen Amine <sup>a,b</sup>, BOUZAZA Abdelkrim <sup>a,b,\*</sup>, MERABET Smail<sup>c</sup>, WOLBERT Dominique <sup>a,b</sup>

<sup>a</sup> Laboratoire Sciences Chimiques de Rennes - équipe Chimie et Ingénierie des Procédés, UMR 6226 CNRS

ENSCR, 11 allée de Beaulieu, 35700 Rennes, France.

<sup>b</sup> Université Européenne de Bretagne. Rennes, France

<sup>c</sup> Laboratoire d'Hydraulique Appliquée et Environnement, Université A. Mira, 06000 Bejaïa, Algeria

\* Corresponding author. Tel.: +33 2 23238056; fax: +33 2 23238120.

E-mail address: [Abdelkrim.bouzaza@ensc-rennes.fr](mailto:Abdelkrim.bouzaza@ensc-rennes.fr) (A.Bouzaza).

## **Abstract**

This paper deals with photocatalysis (TiO<sub>2</sub>+UV), nonthermal plasma (NTP) and their combinations have been widely studied for isovaleraldehyde (Isoval) treatment. Isoval removal, selectivity of CO<sub>2</sub> and CO, and ozone formation are investigated in order to evaluate the performance of the combined process. The results show that the performance of the process has enhanced and a synergetic effect is observed.

On the other hand, this work aims at investigating kinetic modeling of combined process with taking into account the mass transfer step. The model is based on mass balances in three types of region: bulk region, discharge zone and solid phase which contains the photocatalyst. The oxidation in discharge and solid phases is described in two stages. Firstly, the removal of Isoval gives an equivalent intermediate (EI). Secondly, EI is oxidized in to carbon dioxide (CO<sub>2</sub>) and carbon monoxide (CO). This simplified approach of removal allows for an agreement between modeling and empirical data in terms of degradation and mineralization. It also allows for the simulation of NTP and photocatalytic kinetics without knowing the plausible pathway.

Moreover, the synergetic effect can be represented correctly by increasing mass transfer constant.

## **Keywords**

Kinetic modeling; plasma; photocatalysis; synergetic effect; continuous reactor; mass transfer

## **Introduction**

The harmful effects of pollution on the environment and health have led in recent decades and in many countries, to regulate the environmental policies aimed at the reduction of pollution (including air pollution) [1, 2]. It is therefore necessary to reduce emissions, or to treat with economically and environmentally-sustainable technologies [3]. Nonthermal plasma (NTP) is one of technologies which is used to air pollution control. It is about electrical discharge to treat gas present between electrodes separated by a dielectric material, which can ionize the gas, modifying the components [4]. It is characterized by the formation of electrons, ions and neutral molecules [4] which interact and degrade organic compounds such as trimethylamine [6] and toluene [7]. On the other side, a close look to the papers published on the modeling of oxidation process and mass transfer of pollutant in discharge zone shows that it is generally quite difficult to describe NTP. In fact, the majority of published models didn't take into account mass transfer step between bulk and plasma regions so they ignore the effect of mass transfer [9].

Moreover, photocatalysis has been developed toward VOC treatment for several years. This technology has already shown its efficacy toward air pollution. Titanium dioxide ( $\text{TiO}_2$ ) is one of the most investigated photocatalyst for VOC treatments [10]. It is activated by photons provided by an ultra violet (UV) radiation [10-12]. Many studies showed that photocatalysis is a promising process for remediation of air polluted by VOCs [11-13].

On other hand, some other investigations have combined non-thermal plasma with heterogeneous catalysis in the abatement of VOCs at scale laboratory [5, 14]. It is well established now that combined process improves the removal of pollutants [15]. Although many studies has been found a synergetic effect between NTP and  $\text{TiO}_2+\text{UV}$ , the raison for this synergetic has not been extensively explored.

The aim of this study is to evaluate the efficiency of NTP and photocatalysis processes for Isoval removal in planar reactor. Isovaleraldehyde is chosen as representative of odorous compounds [16]. Additionally, the present work deals with the modeling of isovaleraldehyde removal and byproducts formation by coupled NTP+ $\text{TiO}_2+\text{UV}$  in two different continuous reactors: cylindrical and planar without knowing all the intermediate byproducts and the pathway removal.

## **2. Materials and methods**

### **2.1. Reactor design and setup details**

The cylindrical reactor (Fig.1) is principally constituted by two concentric cylinders ( $\text{Ø}58$  and  $76$  mm). To generate the NTP, the reactor is covered by a copper grid which constitutes the outside electrode. The inner electrode is made from a continuous helical aluminum winding. The dielectric media, glass reactor wall, is  $4$  mm thickness. The applied voltage is about  $30$  kV/ $40$  mA and is a sine waveform. It is delivered by a TREK\_30kV high voltage amplifier coupled with a generator BFi OPTILAS. The outside electrode is connected to the ground through a  $2.5$  nF capacity. A digital oscilloscope (Lecroy Wave Surfer 24 Xs,  $200$  MHz) is used in order to visualize the applied voltage and the voltage across the capacity (Fig.1).

The catalytic material consists of a Glass Fiber Tissue (GFT) coated with  $13 \text{ g.m}^{-2}$  of colloidal silica to ensure the fixation of  $13 \text{ g/m}^2$  of titanium dioxide nanoparticles (PC500 Millennium). More details of preparation process are presented in Ahlstrom Patent [17]. The GFT is maintained on the inner reactor wall by the wire electrode (Fig.1). Thus, plasma is directly generated on catalyst surface. An 80W UV lamp is placed in the inner concentric cylinder in order to have a uniform irradiation (fig.1). The UV intensity is equal to  $20 \pm 3 \text{ W.m}^{-2}$ .

**Fig 1: Cylindrical reactor and plasma experimental set-up**

The planar reactor is 1m length and it consists of a rectangular cross section and contains two plates which carried the medium and the electrodes (Fig.2). More descriptions have been detailed in our previous works [14].

**Fig.2: sectional drawing (a) and Schema (b) of NTP coupled with photocatalysis in planar reactor.**

## 2.2. Apparatus and Analysis

To analyze pollutant, a FISIONS Gas chromatograph coupled with a flame ionization detector (GC-FID) is used as described in previous study [18]. The carbon dioxide concentrations are measured by an infrared detector (100 Cosma Beryl ®, Cosma ®, Igny, France). CO concentrations are measured by a CO\_ZRE gas analyzer. Standard iodometric titration method was used to estimate the downstream ozone formation [14].

## 3. Results and discussion

The measurements of isovaleraldehyde removal, the amount of ozone generated and the selectivity of CO and CO<sub>2</sub> were carried out in three configurations: TiO<sub>2</sub>+UV, NTP and NTP+TiO<sub>2</sub>+UV.

The operational conditions/parameters used for the experimental series as well as the evaluation of reactor performance were:

- Inlet ( $C_{inlet}$ ) and outlet ( $C_{outlet}$ ) concentration of pollutant ( $mg \cdot m^{-3}$ )
- Removal capacity ( $RC; mg \cdot h^{-1}$ ) =  $(C_{inlet} - C_{outlet}) \cdot Q$
- Specific energy ( $SE; J \cdot L^{-1}$ ) =  $(P (W) / Q(m^3 \cdot s^{-1})) / 1000$

where Q is the flowrate and P is input power adjusted by changing the applied voltage ( $U_a$ ).

### 3.1. Removal capacity

Using planar reactor, we note that Isoval removal by NTP+TiO<sub>2</sub>+UV is about 5 to 15 % higher than the sum of the capacity recorded, under the same conditions, for NTP and photocatalysis alone. This behavior has been well described in previous study with cylindrical reactor [18]. It is interesting to show that this synergetic effect was observed under various experimental conditions (Fig.3) and it may be explored to the improvement of mass transfer step at solid zone due to turbulence generated by NTP [14].

**Fig. 3: Isoval removal capacity by coupled process vs. the sum of removal capacity of NTP and photocatalysis at different reactor geometries and specific energy**

### 3.2. By-products formation

By-products due to each process using a planar reactor are represented in Fig.4. With coupled process mineralization is improved in comparison with NTP alone (Fig.4). When NTP alone

was used CO<sub>2</sub> selectivity is equal to 17 %. But by adding TiO<sub>2</sub> with external UV, CO<sub>2</sub> selectivity is about 40 %. We note that by photocatalysis alone, the selectivity of CO<sub>2</sub> was around 60 %. In fact, total mineralization by TiO<sub>2</sub> photocatalysis is well-known because the majority of isovaleraldehyde byproducts are transformed into CO<sub>2</sub>. But, with plasma alone, there were many radical reactions which lead to other by-products like CO.

On the other hand, the combined process enhances significantly CO<sub>2</sub> selectivity, in comparison with plasma DBD alone. This enhancement is attributed to the formation of more reactive species due to presence of TiO<sub>2</sub> in plasma discharge zone [21]. Thus the value of mineralization with combined process was an intermediate value between photocatalysis alone and plasma alone.

Moreover, the selectivity of CO was reduced to 7 % with combined NTP and photocatalysis. In the same way, the result shows that the concentration of ozone produced by NTP alone is higher than that due to the NTP+TiO<sub>2</sub>+UV system. This behavior can be explained by the decomposition of ozone in the presence of external UV of planar reactor [5, 18, 19].

**Fig. 4: Variation of amount of ozone, CO and CO<sub>2</sub> selectivity at different processes using planar reactor ( $Q=10 \text{ m}^3.\text{h}^{-1}$ ,  $[\text{Isoval}] = 40 \text{ mg}.\text{m}^{-3}$ ).**

Similar trends were observed with cylindrical reactor at various operating parameters such as relative humidity, inlet concentration and specific energy [18].

#### **4. Modeling of NTP and photocatalysis**

A predicting model which will be able to predict the experimental results is established. The main objective of the model is to permit the reactor design.

## 4.1. Modeling and kinetics

### 4.1.1. Photocatalysis

To describe the photocatalytic oxidation of air pollution, many researchers have used Langmuir-Hinshelwood (L-H) model [13, 22, 23] (eq.1):

$$-r_i = k_{app} \cdot \theta_i = k_{app} \cdot \frac{K_i \cdot C_i}{1 + \sum_{j=1}^n K_j C_j} \quad (1)$$

where  $K_i$  ( $\text{m}^3 \cdot \text{mol}^{-1}$ ) and  $k_{app}$  ( $\text{mol} \cdot \text{m}^{-3} \cdot \text{s}^{-1}$ ) are the apparent constants of model L-H,  $C_i$  ( $\text{mol} \cdot \text{m}^{-3}$ ) is the initial concentration of VOC and  $\theta$  is the fractional surface coverage which can be described as:

$$\theta = \frac{q_i}{q_{m,i}} \quad (2)$$

Where  $q_{m,i}$  ( $\text{mol} \cdot \text{g}^{-1}$ ) and  $q_i$  ( $\text{mol} \cdot \text{g}^{-1}$ ) are respectively the maximum capacity of adsorption and the adsorption capacity onto  $\text{TiO}_2$ .

Only few models have considered a mass transfer step between bulk and solid phase [22, 23]. In fact, Visan et al. [23] have reported an interesting approach to the modeling of PCO reactors based on the light intensity and mass transfer; they model the intrinsic kinetics in immobilized photocatalytic microreactors.

### 4.1.2. Plasma

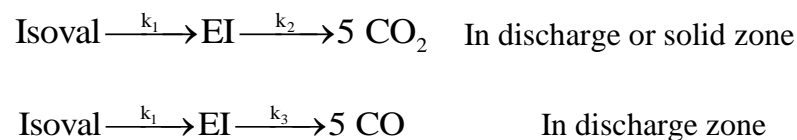
A literature review shows that oxidation modeling of NTP reactors has been explored extensively [9]. However, in most cases, these studies didn't take account to mass transfer step in oxidation process [9, 24]. In our previous study, we have used a simple model which cannot take byproducts of pollutant into account [6]. This model has been used only to describe the removal of trimethylamine and isovaleric acid with NTP (eq.3):

$$R = k_d C_d \frac{P}{V_{reactor}} = k_d C_d \frac{E_{inj}}{V_{reactor}} \cdot Q = k_d C_d \frac{SE}{\tau} \quad (3)$$

where  $k_d$  the apparent rate constant,  $C_d$  pollutant concentration on discharge phase,  $V_{reactor}$  the reactor volume, SE specific energy and P the discharge power,  $\tau$  the residence time of the pollutant on the NTP reactor and Q the flowrate.

#### 4.2. Mass balance in the reactor

In order to facilitate the modeling, the oxidation process has been carried out in two stages. Firstly, the initial pollutant is oxidized to an equivalent intermediate (EI). Secondly, EI gives  $CO_2$  and CO in discharge phase and  $CO_2$  in solid phase.



The NTP+TiO<sub>2</sub>+UV process can be subdivided into six phases (Fig. 5):

- Transfer of gaseous reactants (pollutant and oxygen) to the discharge zone
- Oxidation reaction on the discharge zone
- Transfer of gaseous reactants and byproducts to the solid phase
- Oxidation reaction in solid phase
- Desorption of gaseous photocatalytic reaction products and byproducts.
- Diffusion of products to bulk phase.

**Fig.5: Elemental mass transfer processes involved with NTP+TiO<sub>2</sub>+UV system**

In order to facilitate the modeling, some simplifying hypotheses have been assumed:

1. The electrical energy is uniformly in the thickness of discharge phase
2. The special concentrations of reactive species are uniforms in discharge zone
3. The mass transfer between the bulk phase and discharge zone is driven by molecular diffusion.

The mass balance in the bulk phase (Eq. (4)) and discharge phase (Eq. (5)) can be written as:

$$-u_b \cdot \frac{\partial C_{b,i}(t,x)}{\partial x} - \frac{\partial C_{b,i}(t,x)}{\partial t} + D_L \frac{\partial^2 C_{b,i}(t,x)}{\partial x^2} + \alpha_b \cdot T_{BP} = 0 \quad (4)$$

$$-\frac{\partial C_i(t,x,z)}{\partial t} - u(z) \cdot \frac{\partial C_i(t,x,z)}{\partial x} + D_i \frac{\partial^2 C_i(t,x,z)}{\partial z^2} - R_{P,i}(t,x,z) = 0 \quad (5)$$

Where  $C_{b,i}$  is the concentration of each compound in bulk phase,  $u_b$  represents the velocity,  $D_L$  is the coefficient of axial dispersion and  $D_i$  is the molecular diffusion of each compound,  $T_{BP}$

is the mass flow rate from the bulk to discharge phase:  $T_{BP} = -D_i \left. \frac{\partial C}{\partial z} \right|_{z=e}$

Moreover,  $u(z)$  the velocity in plasma phase can be expressed as:

$$u(z) = u_b \cdot \left(\frac{z}{e}\right)^2 \quad (6)$$

where  $x$  and  $z$  are the axial and radial dimensions respectively and  $e$  represents the thickness of plasma film.

The boundary and initial conditions are as follows:

$$C_{b,i}(t, x = -\infty) = C_0(t)$$

$$C_{b,i}(t, x = +\infty) = 0$$

The mass balance on the photocatalytic phase (Eq. (7)) can be written as:

$$\frac{\partial q_i(t,x)}{\partial t} + \frac{1}{m_c} \cdot T_{PS} - \frac{1}{m_c} \cdot R_{\varphi,i}(t,x) = 0 \quad (7)$$

$m_c$  is the mass of  $\text{TiO}_2$  ( $\text{g.m}^{-2}$ ).  $T_{PS}$  is the mass flow rate from the discharge to solid phase:

$$T_{PS} = a_v \cdot k_f \cdot (C_i - C_{s,i}) \quad (8)$$

where  $k_f$  mass transfer coefficient.  $a_v$  the medium area per unit volume of the reactor ( $\text{m}^2.\text{m}^{-3}$ ),  $C_{s,i}$  concentration of pollutant on the surface of  $\text{TiO}_2$  ( $\text{mol.m}^{-3}$ ). Considering the Langmuir model, this concentration is at equilibrium with the adsorption capacity  $q_i$  ( $\text{mol.g}^{-1}$ ) (eq.9).

$$C_{s,i} = \frac{\theta_i}{K_i \cdot (1 - \sum_{j=1}^n \theta_j)} \quad (9)$$

where  $K$  is the adsorption constant of Langmuir model .

Using the eq.2 the equation 9 can be written as eq.10:

$$C_{s,i} = \frac{\frac{q_i}{q_{m,i}}}{K_i \cdot (1 - \sum_{j=1}^n \left( \frac{q_j}{q_{m,j}} \right))} \quad (10)$$

### 4.3. Adsorption isotherm

To determinate the adsorption constant of Langmuir model and the maximum capacity of adsorption, some adsorption isotherms of isovaleraldehyde were investigated. In fact,  $q_s$  ( $\text{mol.g}^{-1}$ ) which is the quantity of isovaleraldehyde adsorbed on  $\text{TiO}_2$  can be expressed in Eq. (11):

$$q_s = \frac{C_{inlet} - C_{outlet}}{m_c} \cdot V_{reactor} \quad (11)$$

where  $C_{inlet}$  and  $C_{outlet}$  ( $\text{mol.m}^{-3}$ ) are respectively the inlet and the outlet concentration at equilibrium and  $m_c$  ( $\text{g.m}^{-3}$ ) the quantity of photocatalyst,  $V_{reactor}$  the volume of the batch reactor ( $\text{m}^3$ ). The adsorption constant of Langmuir model and the maximum capacity of adsorption can be determined by linearizing  $C_s/q_s$  versus  $C_s$

$$\frac{C_s}{q_s} = \frac{1}{q_m} \left( C_s + \frac{1}{K} \right) \quad (12)$$

The results are satisfactory fitted by Langmuir model [6]. The obtained value for isovaleraldehyde were  $K = 6.0 \times 10^3 \text{ m}^3 \cdot \text{mol}^{-1}$  and  $q_m = 7.2 \times 10^{-1} \text{ mol} \cdot \text{kg}^{-1}$ .

Additionally, to determinate the adsorption parameters ( $K$ ,  $q_m$ ) of EI we supposed that EI is as a molecule having three carbon atoms  $C_3$  which is intermediate between Isoval ( $C_5$ ) and  $CO_2$  ( $C_1$ ). The adsorption constants ( $K$  and  $q_m$ ) of EI found in literature [29, 30] can be used as equal to  $K = 3.6 \times 10^1 \text{ m}^3 \cdot \text{mol}^{-1}$  and  $q_m = 1.29 \text{ mol} \cdot \text{kg}^{-1}$ .

#### 4.4. Modeling of mass transfer

##### 4.4.1. Between bulk and discharge zone

We assume that convection phenomena are negligible and that mass transfer between the bulk and plasma regions was monitored by diffusion [12, 13]. The correlation of Perry et al. [25] was used to calculate the molecular diffusivity ( $D_m$ ) of each reactant in the air. The correlation is as follows:

$$D_i = \frac{1.43 \times 10^{-3} \times T^{1.75}}{P \left[ (\sum \nu)_{Air}^{(1/3)} + (\sum \nu)_i^{(1/3)} \right]^2} \left( \frac{1}{M_{Air}} + \frac{1}{M_i} \right)^{0.5} \quad (13)$$

where  $T$  the ambient temperature (K),  $P$  is the atmospheric pressure (Pa),  $(\sum \nu)_{Air}$  and  $(\sum \nu)_i$  are the molecular volumes of air and reactant (i), and  $M_{Air}$  and  $M_i$  are the molecular weights of air and "i" ( $\text{g} \cdot \text{mol}^{-1}$ ).

##### 4.4.2. Between discharge and photocatalytic zone

In a heterogeneous reaction sequence, mass transfer of reactants first takes place from the discharge phase to the external surface of the TiO<sub>2</sub> particles. The reactants then diffuse from the external surface into and through the pores within the TiO<sub>2</sub> particles, with reaction taking place only on the catalytic surface of the pores.

But, many studies [14, 22, 23] neglect the internal mass transport inside the pores. Hence, the reaction rate is set as the boundary condition for the catalyst–fluid interface. Thus, to determine the constant of external mass transfer  $k_m$ , several correlations were used. In fact, using the planar reactor,  $k_m$  can be determined by semi-empirical correlations [26]:

$$Sh = 0.664 (Re)^{(1/2)} \cdot (Sc)^{(1/3)} \quad (15)$$

For laminar flow in cylindrical reactor,  $k_m$  is calculated using a correlation detailed by Mobarak et al. [27]:

$$Sh = 1,029 \times Sc^{0.33} \times Re^{0.55} \times \left( \frac{L_{tot}}{d} \right)^{-0.472} \quad (16)$$

where Re, Sc and are respectively Reynolds, Schmidt and Sherwood dimensionless number,  $d$  is the equivalent diameter of cylindrical reactor and  $L_{tot}$  is its length.

More details concerning Reynolds values and  $k_m$  calculations were given in our previous work [8, 12].

## 4.5. Modeling of kinetic reaction

### 4.5.1. In plasma zone

NTP is generated in air where N<sub>2</sub> and O<sub>2</sub> are the main constituents. To simplify the oxidation process, the model takes into account only one species: atomic oxygen [9, 24, 28].

The electron concentration, averaged over several cycles, can be considered proportional to a power of the specific energy:

$$C_{e^-} = \alpha \cdot E_Z^{\alpha_{E,1}} \quad (17)$$

The reaction between electrons and oxygen can be written as follows:

$$r = -k \cdot C_{e^-} \cdot [O_2] = -k' \cdot E_Z^{\alpha_{E,1}} \cdot [O_2] \quad (18)$$

It is generally accepted that the plasma removal rate can be modeled by the general expression (eq.19):

$$R_{P,i}(t, x, z) = \sum_{j=1}^{n_r} \vartheta_{i,j} \cdot k_j \cdot E_Z^{\alpha_{E,j}}(t) \cdot \prod_{p=1}^{n_c} C_i^{\gamma_{p,j}}(t, x, z) \quad (19)$$

where  $R_p$  is the removal rate in plasma phase, SE the specific energy of plasma,  $C_i$  the concentration of each compound in the plasma layer,  $k_j$  the constant rate,  $t$  time (min),  $z$  the distance which is perpendicular to flow in plasma zone (film thickness) (m),  $x$  the distance in the flow direction (m).

$\vartheta_{i,j}$  are stoichiometric coefficients of the removal reaction,  $\alpha_{E,j}$ ,  $\gamma_{p,j}$  orders of reaction,  $n_c$  and  $n_r$  number of compounds and reactions respectively.

#### 4.5.2. In photocatalytic zone

Here, in order to simplify the modeling work, relative humidity and UV intensity, are kept constant.

Using L-H model, basic equation of the photocatalytic degradation kinetics of compound  $i$  can be written as:

$$R_i = k_j \cdot f(I) \cdot \prod_j q_j^{n_j} \quad (20)$$

where

$$q_j = q_{m,j} \cdot f(C_j) \quad (21)$$

The photocatalytic oxidation is then expressed by Eq (20).

$$R_i(t, x) = \sum_{j=1}^{\varphi} \vartheta_{i,j} \cdot k_j \cdot I(t)^{\gamma_I} \cdot \left( \frac{K \cdot C(t, x, 0)}{1 + \alpha \cdot I(t) + K \cdot C(t, x, 0)} \right)^{\gamma_{p,i}} \cdot \prod_{p=1}^{n-1} \theta_p^{\gamma_{p,j}}(t, x) \quad (22)$$

where I is the UV intensity of lamp,  $\theta_p$  the fractional surface coverage, C the concentration of each compound adsorbed on the solid phase, k and K L-H constants, and  $\vartheta_{i,j}$  the stoichiometric coefficients.  $\gamma_{p,i}$ ,  $\gamma_I$  and  $\gamma_{p,j}$  are orders of reaction,  $\varphi$  and  $n_p$  are respectively number of compounds and reactions,  $\alpha$  coefficient of UV intensity.

Boundary and initial conditions are as follows:

$$C_i(0, x) = C_0$$

$$q(0, x) = 0$$

## 5. Simulation procedure

Equations (4) to (20) were incorporated into a program in Fortran ® language which was written with the main objective of flexibility. In fact, we wanted to have the possibility to vary the main parameters (specific energy, concentration, flow rate) or to change the geometry reactor with plasma alone, photocatalysis and combined process UV and to provide a more detailed description or less complex chemical mechanisms.

A step of comparing our various experimental results and simulations from the same operating conditions will allow us to access the values of certain parameters and kinetic constants and thus to validate the choice of a reaction mechanism.

The incoming flow is defined by the nature and concentration of these compounds, as well as by the parameters of the effluent. The program reads the data in three input files: ".Fed" extensions containing parameters and fluid ".Prd" containing the data of seven compounds and the various constants and their reactions which their number was nine are supplied by a file ".Rea" Additionally, the resolution of the partial differential equation set is carried out by using orthogonal collocation. The simulations were done with Neosim/Excel. It gives the outlet concentration of isoval and the formed byproducts at different specific energy and flow rate using planar and cylindrical reactors. A Gauss-Newton method is carried out to determine the values of kinetics constants ( $k_j$ ), by a least square fitting of the difference between simulated and empirical results [23].

### 5.1. NTP

Fig. 6 shows the evolution of the isovaleraldehyde transitory concentration and some products with the time resulting from NTP reaction. Here, the plasma is switched ON after 20 min. After this period, Fig.6 shows that all the concentrations of byproducts are stable. On the other hand, experimental data have been represented on the same figure after 2 hours which was the experimental time for checking experimental point.

After optimization, the numerical resolution [29] gives outlet isovaleraldehyde concentration, selectivity of  $\text{CO}_x$  and amount of ozone at different operating parameters of each geometry of reactor and at each inlet concentration.

The values of constants  $k_1$ ,  $k_2$ ,  $k_3$  and  $k(\text{O}_3)$  are summarized in Table 1.

**Table 1: Values of constants**

The comparison between experimental and predicted results is represented on Fig. 6. Here, we represent only the result simulation with the planar reactor. The model describes reasonably well the removal of isovaleraldehyde. The description of the degradation kinetics by a model with a single EI is able to reproduce the plasma oxidation process.

Regarding byproducts formation, the predicted result is also satisfying during the study. The model is accurate, but tends to underestimate the ozone formation. Indeed, it is known that the formation of ozone is based on recombination reaction between oxygen molecule and atomic oxygen. The model only takes into account one active specie ( $O^\circ$ ); this behavior leads to a decrease of oxygen atomic amount resulting to a reduction of ozone formation. Thus, this effect can probably explain the underestimate of the ozone formation (Fig.6).

**Fig.6: Experimental and simulated results of Isoval outlet concentration and byproducts formation vs. time using planar reactor (Process: Plasma alone  $[Isoval]_0=40 \text{ mg}\cdot\text{m}^{-3}$ ,  $Q=10 \text{ m}^3\cdot\text{h}^{-1}$ ,  $SE=14 \text{ J}\cdot\text{L}^{-1}$ ,  $T=20^\circ\text{C}$ ,  $HR=50\%$ )**

It is interesting to mention that this model gives also, overall, satisfactory results with cylindrical reactor. The results with this reactor are not represented here.

## 5.2. Photocatalysis

In Fig. 7, it is shown that the variation of transitory Isoval concentration and products have resulted from photocatalytic reaction with time. After 80 min of contact, UV lamp are kept OFF, the inlet and the outlet concentrations of Isoval are the same which means that the photocatalytic medium is saturated. After this adsorption period, the UV lamp is ON. For a reaction time beyond 30 min, all the concentrations of byproducts are stables. Additionally experimental data have been represented on the same figure for reaction time beyond 150 min.

As seen on figure 7, the model describes reasonably well the Isoval removal throughout the experiments and for whatever the initial concentration. Regarding the mineralization, the model represents well the CO<sub>2</sub> concentration. But, with high inlet concentration of Isoval, it tends to underestimate the CO<sub>2</sub> formation. It is known that the mineralization of complex organic pollutants occurs via several successive reactions. In fact, there are other pathways of CO<sub>2</sub> formation which probably explains the underestimation of the CO<sub>2</sub> release.

The values of  $k_4$  and  $k_5$  are summarized in Table 2. These constants ( $k_4$  &  $k_5$ ) (see table 2) are similar to those obtained for hexanal removal by Vuong and co-workers [30].

**Table 2: Values of kinetic coefficients**

**Fig.7: Experimental and simulated results of Isoval outlet concentration and byproducts formation vs. time using planar reactor: empty symbol = experimental data at [Isoval]<sub>0</sub>= 40 mg.m<sup>-3</sup> and full symbol = experimental data at [Isoval]<sub>0</sub>= 15 mg.m<sup>-3</sup> (Process: photocatalysis alone, Q= 10 m<sup>3</sup>.h<sup>-1</sup>, SE=14 J.L<sup>-1</sup>, T=20°C, HR=50%)**

The simulation data using cylindrical reactor are not reported. Therefore, we note that the model correlate experimental results satisfactory.

### **5.3. Modeling and simulation of combined process (NTP+TiO<sub>2</sub>+UV)**

When we simulate the coupled process, we used the constants obtained previously (Tables 1 and 2). Thus predicted results were not consistent with empiric data (not represented).

So, for having a better fitting, we conducted to adjust the flow of mass transfer between discharge and photocatalysis zones. Indeed, the presence of the turbulences generated by plasma on the photocatalytic medium can enhance the mass transfer. Moreover when we

increase four times the value of  $k_m$  the model is able to predict the experimental results of coupled NTP and  $\text{TiO}_2+\text{UV}$ . It gives a satisfactory overall description of isovaleraldehyde removal (Fig. 8), mineralization (Fig.9) and ozone formation (Fig.10) using two geometries of reactor.

**Fig.8: Comparison of result of concentration simulated vs. the empirical data at different flow rates and inlet concentrations with coupled process.**

**Fig.9: Comparison of  $\text{CO}_2$  selectivity simulated vs. the empirical data at different specific energy with coupled process.**

**Fig.10: Comparison of ozone concentration simulated vs. the empirical data at different specific energy with coupled process.**

The values of constants  $k_{m,1}$  and  $k_{m,2}$  when photocatalysis is used alone and in combination with NTP are summarized in Table 3.

**Table 3: values of mass transfer constants**

Otherwise, we propose that the existence of a synergetic effect, when the two processes are combined. Thus, by increasing the mass transfer constant, the model is able to take into account the synergetic effect due to process combination (Fig 8-10).

## **6. Conclusion**

In this paper, the efficient removal of isovaleraldehyde has been demonstrated by coupling NTP and photocatalysis. The oxidation process has been implemented in annular and planar reactors. There have been three improvements observed that are (i) a synergetic effect on the removal of isovaleraldehyde (ii) an improvement in the mineralization (iii) reduction on ozone formation.

A kinetic model taking into account mass transfer step is developed. To improve the model, the plausible pathway is simplified and supposed to occur on two stages. Firstly Isoval gives an equivalent intermediate (EI). Then on a second stage, EI gives CO<sub>2</sub> and/or CO.

The developed model describes successfully the removal of isovaleraldehyde by NTP, photocatalysis and coupled process. Moreover, mineralization and the amount of ozone formed were well simulated by the model.

In other hand, synergetic effect is easily taken into account by acting on the mass transfer coefficient.

## References

[1] Council of Europe Council, Directive 1999/13/EC on the limitation of emissions of volatile organic compounds due to use of organic solvents in certain activities and installations, Official Journal of the European Union, 1999, L85, 1.

- [2] USA EPA, Clean Air Act. US Code, Environmental Protection Agency, Washington, DC, 2008.
- [3] European Solvent Industry Group (ESIG), 2009, Available on-line. <http://www.esig.org> Accessed, 11 November 2012.
- [4] M. Capitelli, 1965. Plasma Kinetics in Atmospheric Gases, New York -Springer.
- [5] J. Taranto, D. Frochot, P. Pichat, Combining Cold Plasma and TiO<sub>2</sub> Photocatalysis To Purify Gaseous Effluents: A Preliminary Study Using Methanol-Contaminated Air, *Ind. Eng. Chem. Res.* 46 (2007) 7611-7614.
- [6] A.A. Assadi, A. Bouzaza, M. Lemasle, D.Wolbert, Removal of trimethylamine and isovaleric acid from gas streams in a continuous flow surface discharge plasma reactor, *Chemical engineering research and design*. *In press*.
- [7] H. Huang, D. Ye, D. Y. C. Leung, Abatement of Toluene in the Plasma-Driven Catalysis: Mechanism and Reaction Kinetics, *IEEE transactions on plasma science* 39 (2011) 877-882.
- [8] A.A. Assadi, J. Palau, A. Bouzaza, D.Wolbert, Modeling of a continuous photocatalytic reactor for isovaleraldehyde oxidation: Effect of different operating parameters and chemical degradation pathway, *chemical engineering research and design* 91 (2013) 1307–1316
- [9] Y. S. Mok, W. Lee Ho, Y. J. Hyun, S. W. Ham, I. S. Nam, Determination of Decomposition Rate Constants of Volatile Organic Compounds and Nitric Oxide in a Pulsed Corona Discharge Reactor, *Korean J. Chem. Eng* 18 (2001) 711-718.
- [10] P. Pichat, Some views about indoor air photocatalytic treatment using TiO<sub>2</sub>: Conceptualization of humidity effects, active oxygen species, problem of C<sub>1</sub>–C<sub>3</sub> carbonyl pollutants, *Applied Catalysis B: Environmental* 99 (2010) 428–434.
- [11] P. Pichat, J. Disdier, C. Hoang-Van, D. Mas, G. Goutailler, C. Gaysse, Purification/deodorization of indoor air and gaseous effluents by TiO<sub>2</sub> photocatalysis, *Catalysis Today* 63 (2000) 363–369.

- [12] A.A. Assadi, A. Bouzaza, D. Wolbert, Photocatalytic oxidation of Trimethylamine and Isovaleraldehyde in an annular reactor: Influence of the Mass Transfer and the relative humidity. *Journal of Photochemistry and Photobiology A: Chemistry* 236 (2012) 61–69.
- [13] A. Bouzaza, C. Vallet, A. Laplanche, Photocatalytic degradation of some VOCs in the gas phase using an annular flow reactor: determination of the contribution of mass transfer and chemical reaction steps in the photodegradation process. *Journal of Photochemistry and Photobiology A: Chemistry*. 177 (2006) 212–217.
- [14] A. A. Assadi, J. Palau, A. Bouzaza, J. Peña-Roja, V. Martínez-Soria, D. Wolbert, Abatement of 3-methylbutanal and trimethylamine with combined plasma and photocatalysis in a continuous planar reactor, *Journal of Photochemistry and Photobiology A: Chemistry* 282 (2014) 1–8.
- [15] C. Subrahmanyam, M. Magureanu. D. Laub, A. Renken, L. Kiwi-Minsker, Nonthermal plasma abatement of trichloroethylene enhanced by photocatalysis. *Journal of physical chemistry. C* 111 (2007) 4315–4318.
- [16] International Programme on Chemical Safety (IPCS), OECD screening information databases 3-methylbutanal. UNEP, Canadian Centre for Occupational Health and Safety (CCOHS), 2004.
- [17] Ahlstrom Patent EP 1069950, 2000. AU 735798 US 09/467, 650; JP 2000-542104.
- [18] A.A. Assadi, A. Bouzaza, D. Wolbert, Use of DBD plasma, photocatalysis, and combined DBD plasma/photocatalysis in a continuous annular reactor for isovaleraldehyde elimination - synergetic effect and byproducts identification. *Chemical Engineering Journal* 254 (2014) 124–132
- [19] L. Sivachandiran, F. Thevenet, A. Rousseau, Non-Thermal Plasma Assisted Regeneration of Acetone Adsorbed TiO<sub>2</sub> Surface, *Plasma Chem Plasma Process* 33 (2013) 855–871.
- [20] L. Sivachandiran, F. Thevenet, A. Rousseau, Regeneration of isopropyl alcohol saturated Mn<sub>x</sub>O<sub>y</sub> surface: Comparison of thermal, ozonolysis and non-thermal plasma treatments, *Chemical Engineering Journal* 246 (2014) 184–195.

- [21] A.S. Besov, A.V. Vorontsov, Acceleration of Acetone Destruction Process under Synergistic Action of Photocatalytic Oxidation and Barrier Discharge, *Plasma Chemistry and Plasma Processing* 27 (2007) 624–634.
- [22] S. Brosillon, L. Lhomme, Wolbert D. Modelling of a falling thin film deposited photocatalytic step reactor for water purification: Pesticide treatment, *Chemical Engineering Journal* 169 (2011) 216–225.
- [23] A. Visan, D. Rafieian, W. Ogieglo, R. G.H. Lammertink, Modeling intrinsic kinetics in immobilized photocatalytic microreactors, *Applied Catalysis B: Environmental*, 150–151 (2014) 93–100.
- [24] N. Aggadi, X. Duten, Ph. Marteau, M. Redolfi, K. Hassouni : "n-hexane soot oxidation in N<sub>2</sub>/O<sub>2</sub> and N<sub>2</sub>/O<sub>2</sub>/NO<sub>2</sub> atmospheric pressure pulsed corona discharges", *Eur. Phys. J. Appl. Phys.* 36 (2006) 165-175.
- [25] R.H. Perry, D. Green, J.O. Maloney, 1997. *Perry's chemical engineers's handbook*, 7<sup>th</sup> edition. New-York, Mc Graw-Hill Book Company.
- [26] D. Basmadjian, 2007. *Mass Transfer and Separation Processes: Principles and Applications*, Second edition, University of Toronto, Ontario, Canada.
- [27] A.A. Mobarak, H.A. Farag, G.H. Sedahmed, Mass transfer in smooth and rough annular ducts under developing flow conditions. *Journal of applied electrochemistry*, 27 (1997) 201-207.
- [28] A.M. Vandenbroucke, R. Morent, N. De Geyter, C. Leys, Non-thermal plasmas for non-catalytic and catalytic VOC abatement Review, *Journal of Hazardous Materials* 195 (2011) 30-54.
- [29] Baup S., 2000 - Elimination de pesticides sur lit de charbon actif en grain en présence de matière organique naturelle : élaboration d'un protocole couplant expériences et calculs numériques afin de simuler les équilibres et les cinétiques compétitifs d'adsorption. Thèse de Doctorat, Université de Poitiers.
- [30] Vuong M., 2011- Dépollution et désodorisation de l'air par photocatalyse assistée par adsorption sur charbon actif en réacteur à flux frontal continu et séquence. Thèse de doctorat, Université de Rennes 1.

Table captions

Table 1: Values of constants

| Kinetic constant | $k_1$ ( $\text{m}^3 \cdot \text{mol}^{-1} \cdot \text{s}^{-1}$ ) | $k_2$ ( $\text{m}^3 \cdot \text{mol}^{-1} \cdot \text{s}^{-1}$ ) | $k_3$ ( $\text{m}^3 \cdot \text{mol}^{-1} \cdot \text{s}^{-1}$ ) | $k(\text{O}_3)$ ( $\text{s}^{-1}$ ) |
|------------------|--|--|--|-------------------------------------|
| Values           | $1.21 \cdot 10^{-2}$   | $1.31 \cdot 10^{-2}$   | $5.60 \cdot 10^{-4}$   | $2.70 \cdot 10^{-4}$                |

Table 2: Values of kinetic coefficients

| Kinetic constant    | $K_4$                | $K_5$                |
|---------------------|----------------------|----------------------|
| Values ( $s^{-1}$ ) | $0.63 \cdot 10^{-6}$ | $0.94 \cdot 10^{-6}$ |

Table 3: values of mass transfer constants

| Constant of mass transfer | $k_{m,1} (\times 10^3 \cdot m \cdot s^{-1})$ | $k_{m,2} (\times 10^3 \cdot m \cdot s^{-1})$ |
|---------------------------|--|--|
| Value                     | 4.20   | 16.80  |

### Figure captions

Fig 1: Cylindrical reactor and plasma experimental set-up

Fig.2: sectional drawing (a) and Schema (b) of NTP coupled with photocatalysis in planar reactor.

Fig. 3: Isoval removal capacity by coupled process vs. the sum of removal capacity of NTP and photocatalysis at different reactor geometries and specific energy

Fig. 4: Variation of amount of ozone, CO and CO<sub>2</sub> selectivity at different processes using planar reactor ( $Q=10 \text{ m}^3 \cdot \text{h}^{-1}$ ,  $[\text{Isoval}] = 40 \text{ mg} \cdot \text{m}^{-3}$ ).

Fig. 5: Elemental mass transfer processes involved with NTP+TiO<sub>2</sub>+UV system

Fig.6: Experimental and simulated results of Isoval outlet concentration and byproducts formation vs. time using planar reactor (Process: Plasma alone  $[\text{Isoval}]_0=40 \text{ mg} \cdot \text{m}^{-3}$ ,  $Q= 10 \text{ m}^3 \cdot \text{h}^{-1}$ ,  $SE=14 \text{ J} \cdot \text{L}^{-1}$ ,  $T=20^\circ\text{C}$ ,  $HR=50\%$ )

Fig.7: Experimental and simulated results of Isoval outlet concentration and byproducts formation vs. time using planar reactor: empty symbol = experimental data at  $[\text{Isoval}]_0= 40 \text{ mg} \cdot \text{m}^{-3}$  and full symbol = experimental data at  $[\text{Isoval}]_0= 15 \text{ mg} \cdot \text{m}^{-3}$  (Process: photocatalysis alone,  $Q= 10 \text{ m}^3 \cdot \text{h}^{-1}$ ,  $SE=14 \text{ J} \cdot \text{L}^{-1}$ ,  $T=20^\circ\text{C}$ ,  $HR=50\%$ )

Fig.8: Comparison of result of concentration simulated vs. the empirical data at different flow rates and inlet concentrations with coupled process.

Fig.9: Comparison of CO<sub>2</sub> selectivity simulated vs. the empirical data at different specific energy with coupled process.

Fig.10: Comparison of ozone concentration simulated vs. the empirical data at different specific energy with coupled process.

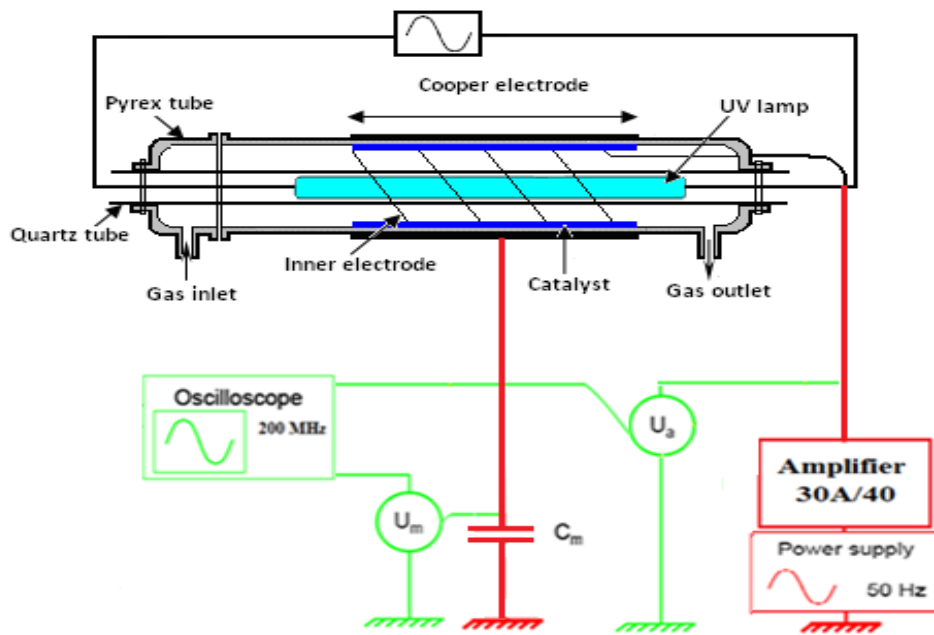


Fig 1: Cylindrical reactor and plasma experimental set-up

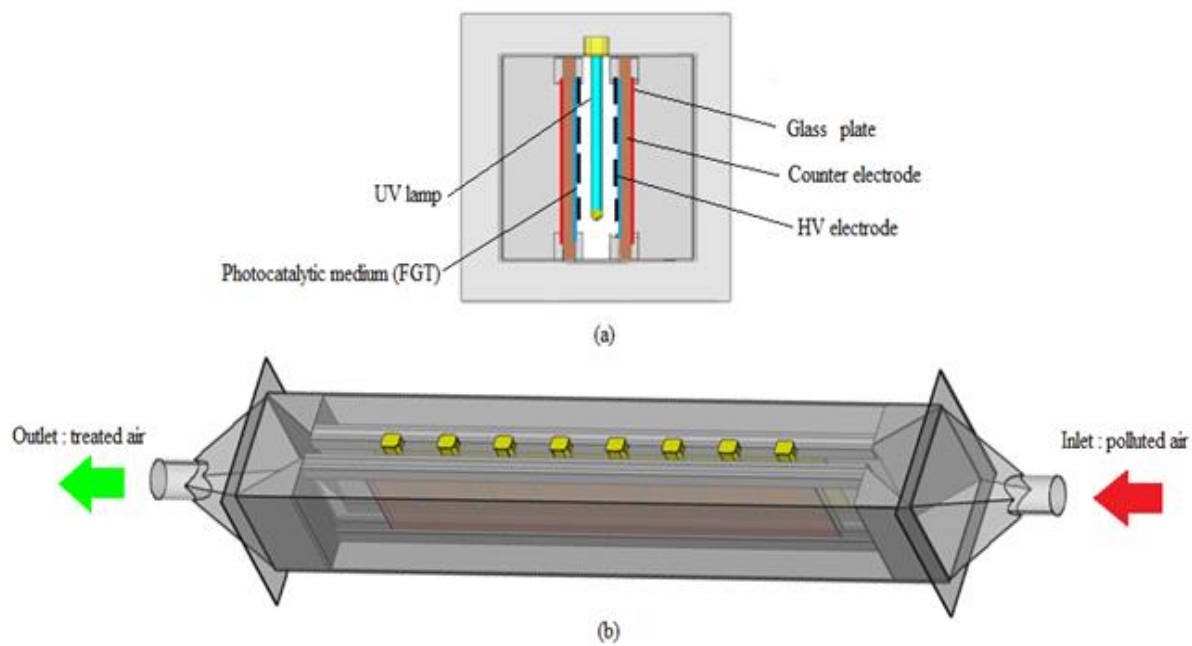


Fig.2: sectional drawing (a) and Schema (b) of NTP coupled with photocatalysis in planar reactor.

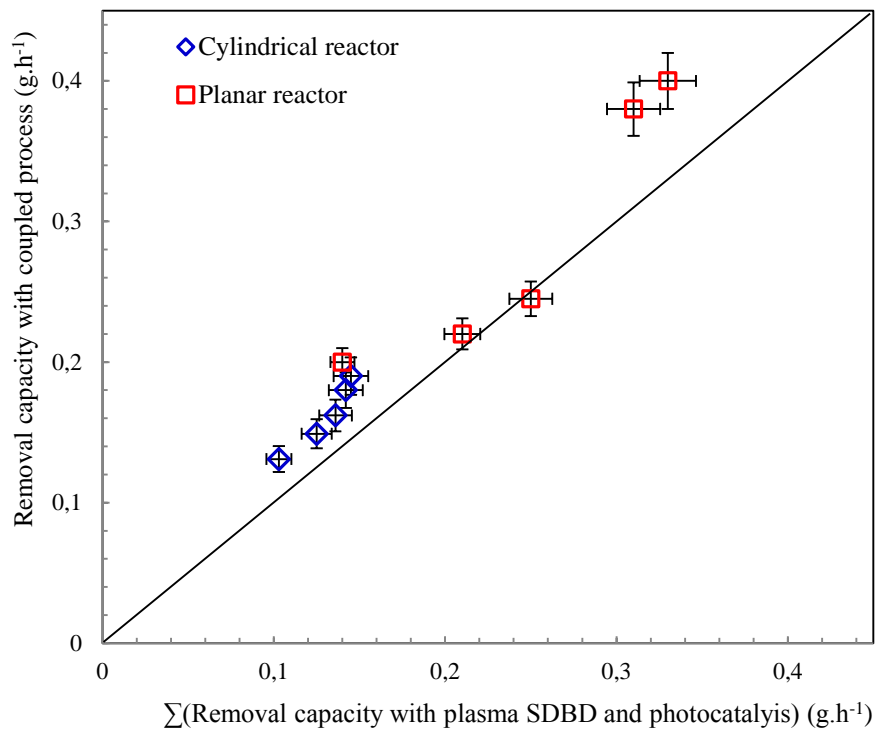


Fig. 3: Isoval removal capacity by coupled process vs. the sum of removal capacity of NTP and photocatalysis at different reactor geometries and specific energy

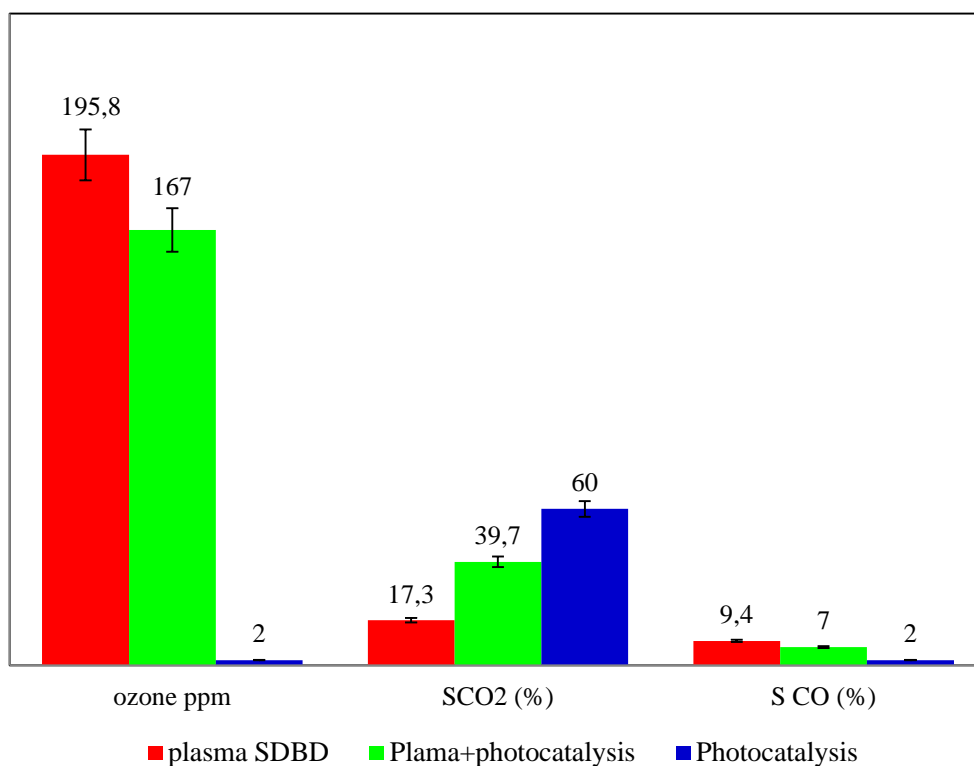


Fig. 4: Variation of amount of ozone, CO and CO<sub>2</sub> selectivity at different processes using planar reactor ( $Q=10 \text{ m}^3 \cdot \text{h}^{-1}$ ,  $[\text{Isoval}] = 40 \text{ mg} \cdot \text{m}^{-3}$ ).

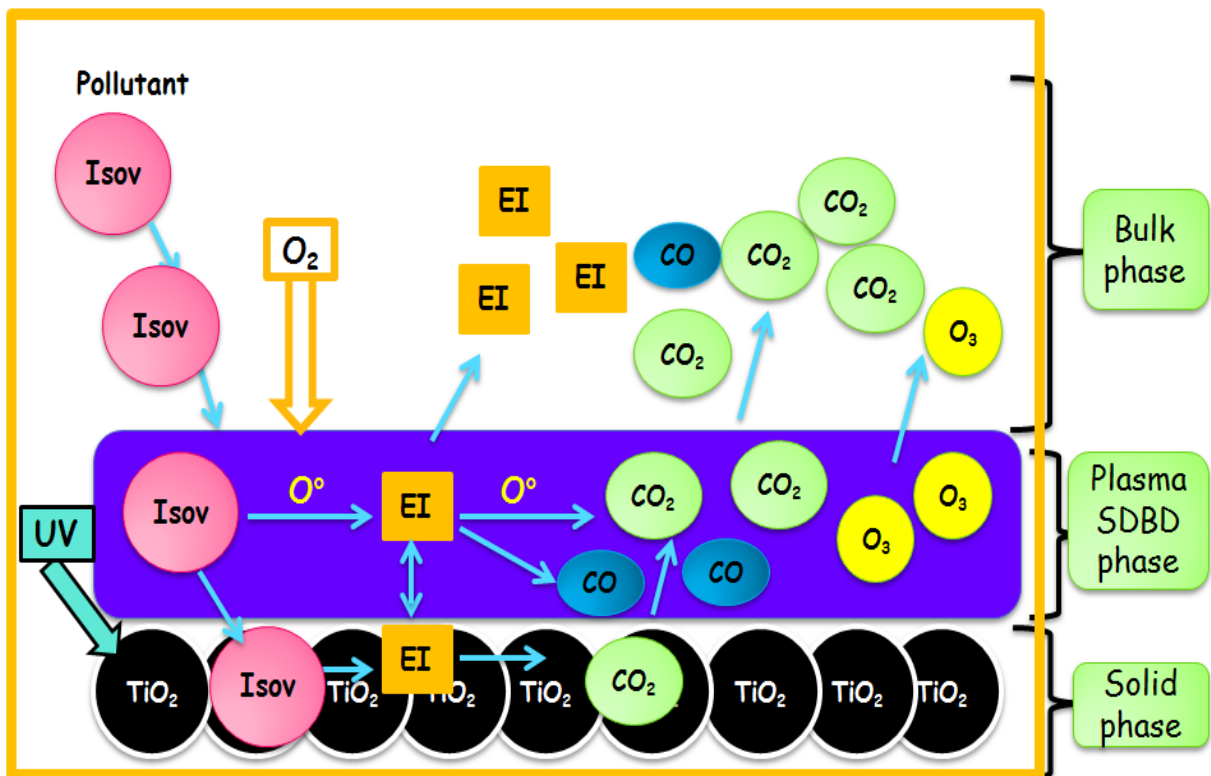


Fig.5: Elemental mass transfer processes involved with NTP+TiO<sub>2</sub>+UV system

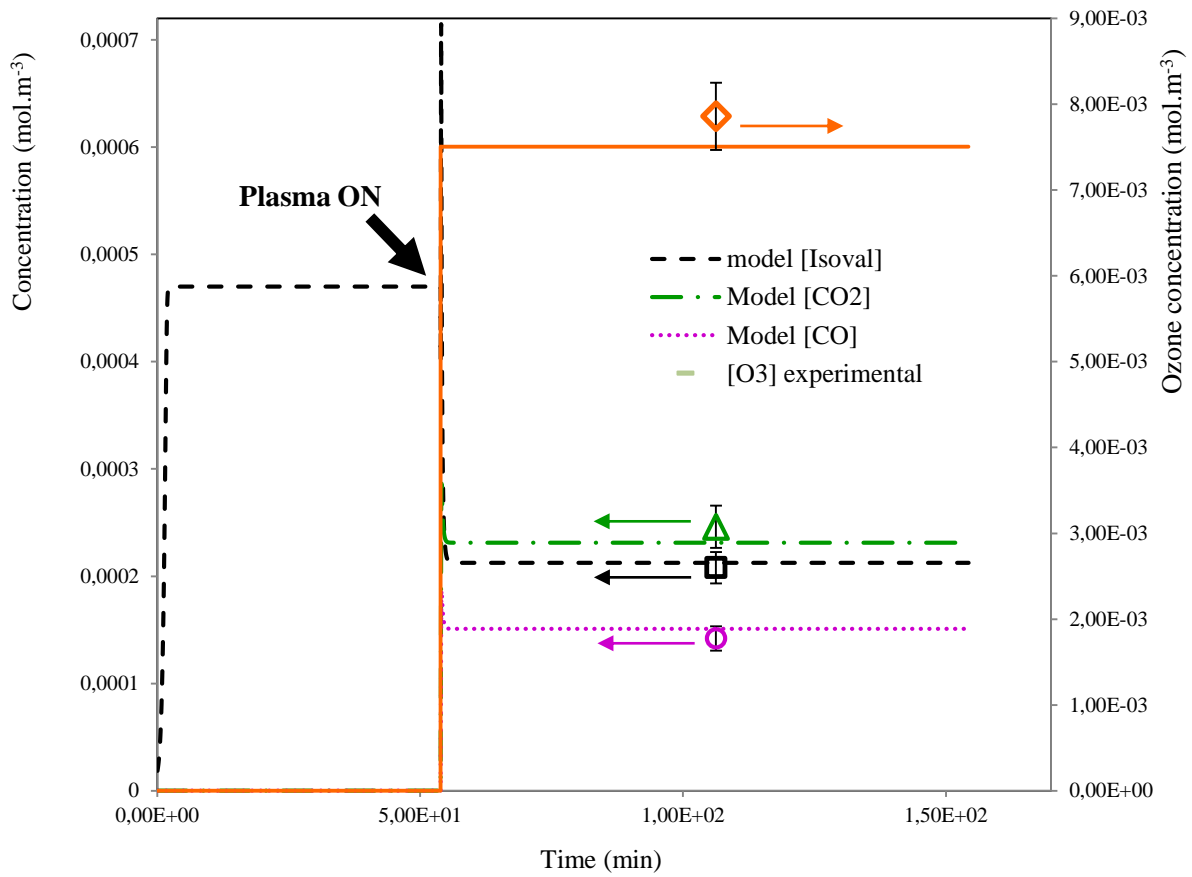


Fig.6: Experimental and simulated results of Isoval outlet concentration and byproducts formation vs. time using planar reactor (Process: Plasma alone  $[Isoval]_0=40 \text{ mg.m}^{-3}$ ,  $Q=10 \text{ m}^3.\text{h}^{-1}$ ,  $SE=14 \text{ J.L}^{-1}$ ,  $T=20^\circ\text{C}$ ,  $HR=50\%$ )

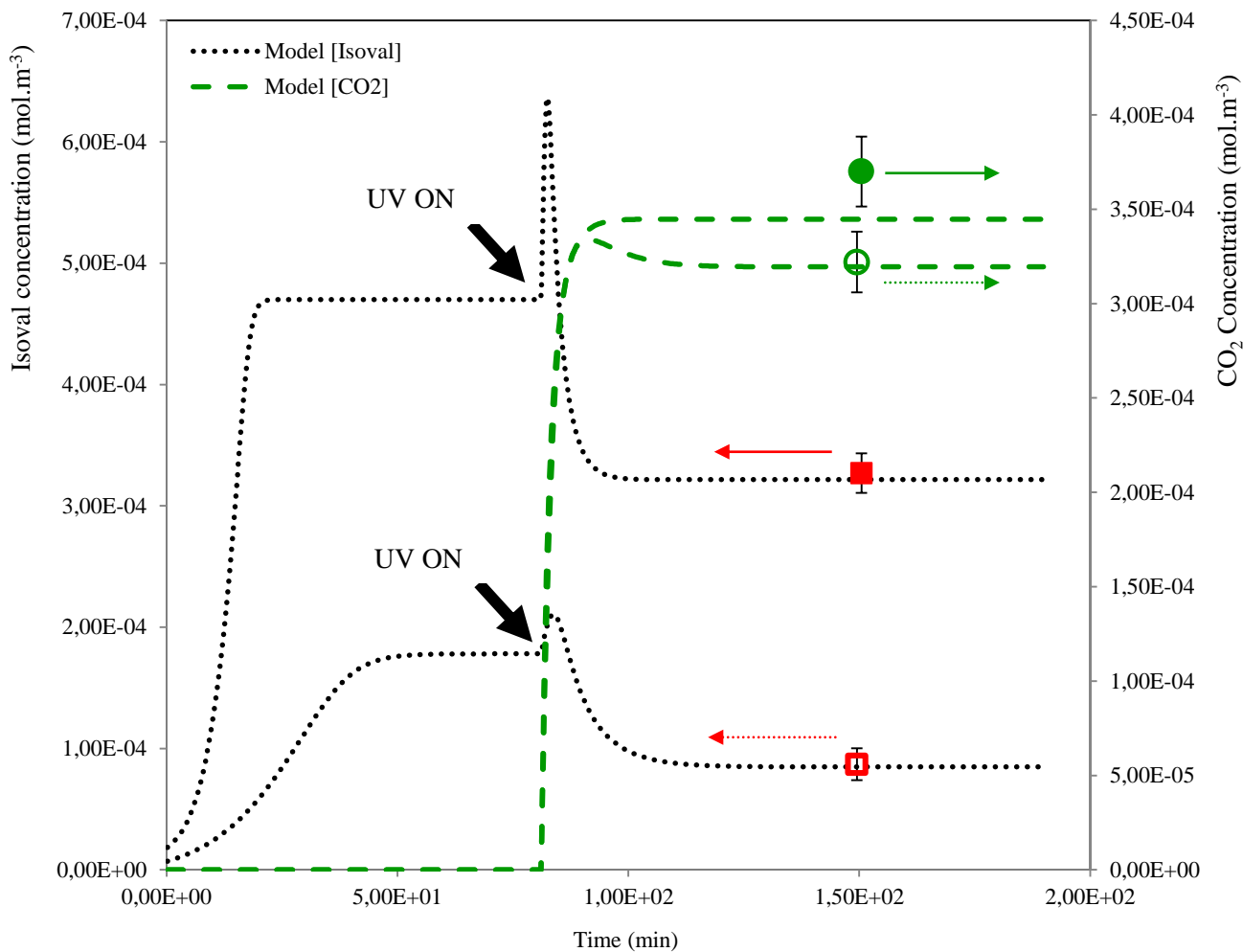


Fig.7: Experimental and simulated results of Isoval outlet concentration and byproducts formation vs. time using planar reactor: empty symbol = experimental data at  $[Isoval]_0 = 40 \text{ mg.m}^{-3}$  and full symbol = experimental data at  $[Isoval]_0 = 15 \text{ mg.m}^{-3}$  (Process: photocatalysis alone,  $Q = 10 \text{ m}^3.\text{h}^{-1}$ ,  $SE = 14 \text{ J.L}^{-1}$ ,  $T = 20^\circ\text{C}$ ,  $HR = 50\%$ )

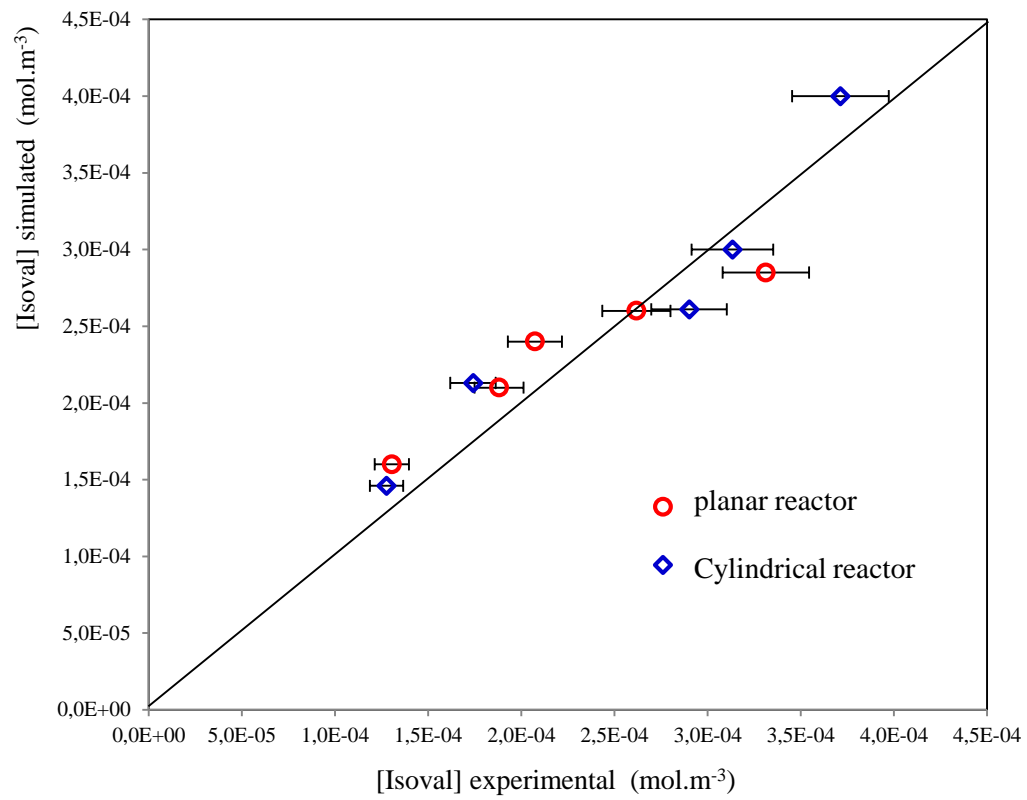


Fig.8: Comparison of result of concentration simulated vs. the empirical data at different flow rates and inlet concentrations with coupled process.

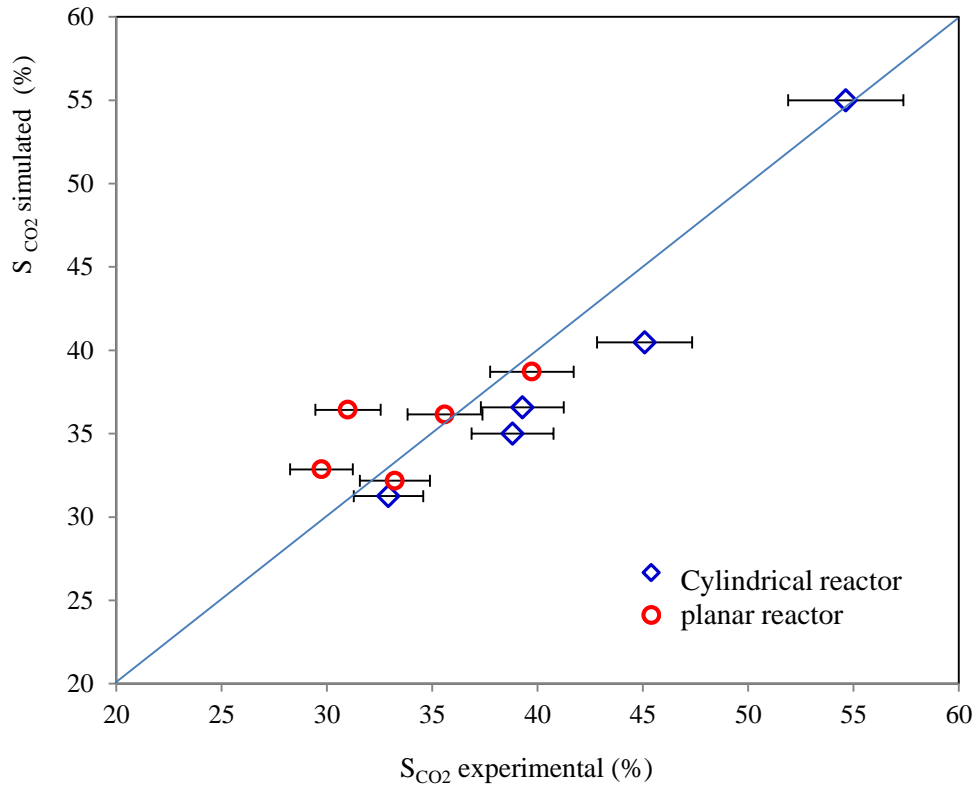


Fig.9: Comparison of CO<sub>2</sub> selectivity simulated vs. the empirical data at different specific energy with coupled process.

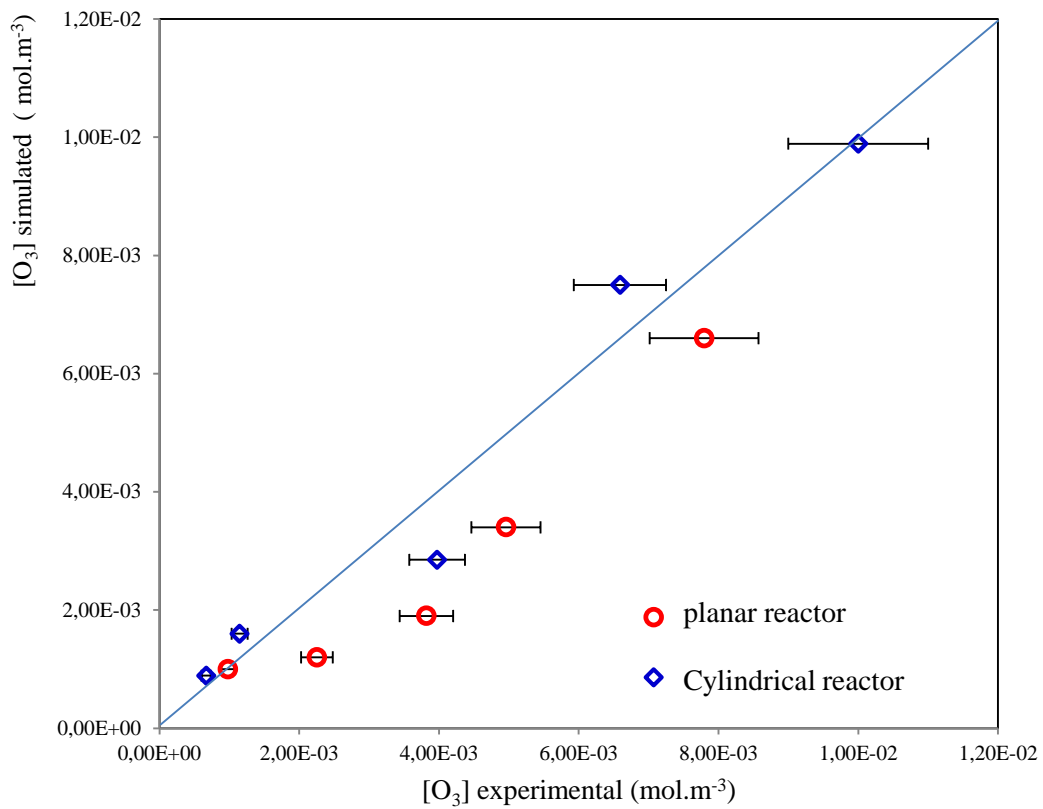


Fig.10: Comparison of ozone concentration simulated vs. the empirical data at different specific energy with coupled process.